Organic Electronics

DOI: 10.1002/ange.201209999

Transferable Graphene Oxide by Stamping Nanotechnology: Electron-Transport Layer for Efficient Bulk-Heterojunction Solar Cells**

*Dong Hwan Wang, Jung Kyu Kim, Jung Hwa Seo, Insun Park, Byung Hee Hong, Jong Hyeok Park, and Alan J. Heeger**

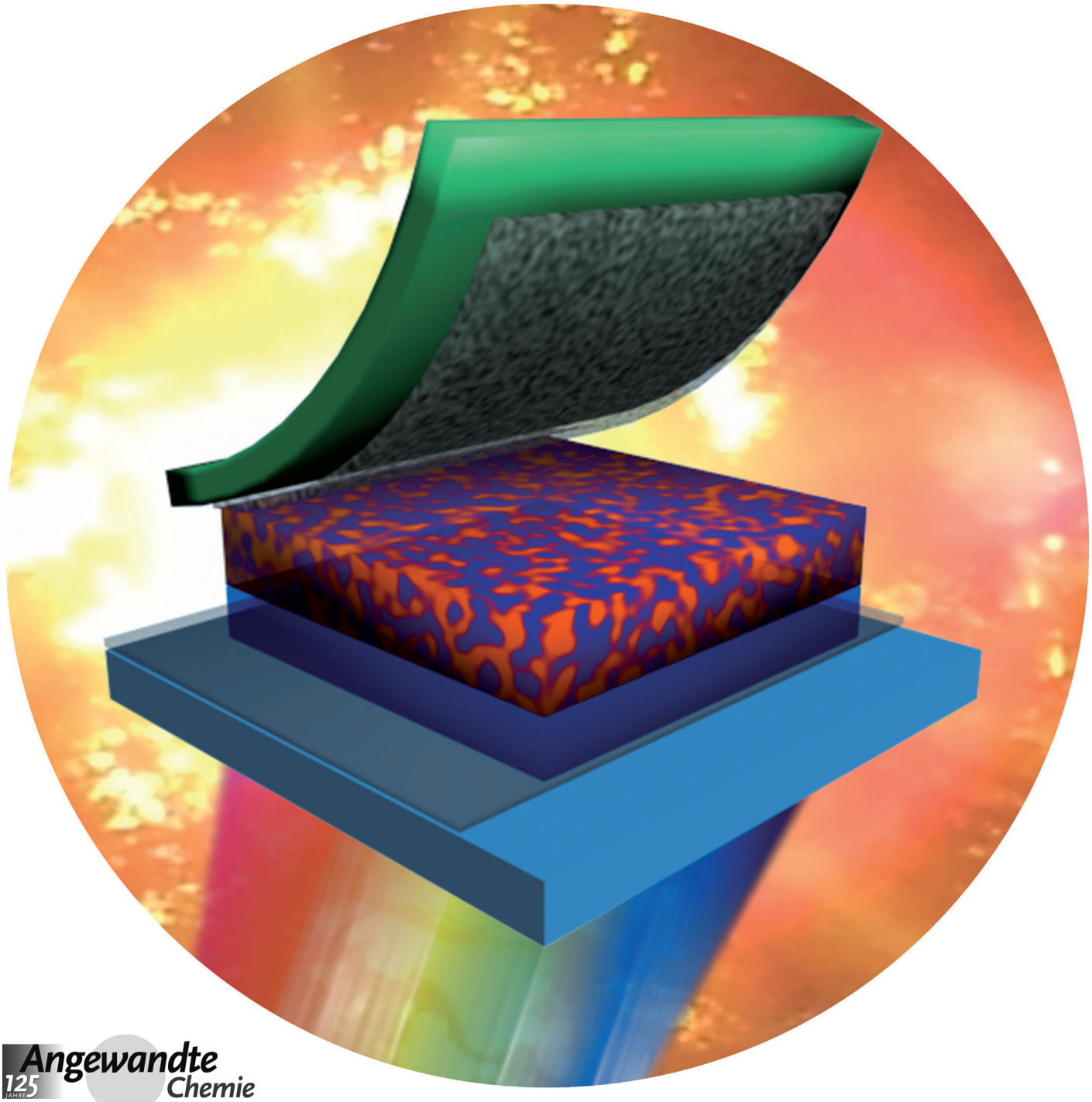

Donor–acceptor-blended bulk-heterojunction (BHJ) solar cells fabricated by low-cost printing technology offer a number of advantages: They are robust, lightweight, and flexible and can be produced in large area by roll-to-roll manufacturing.[1–4] During recent years, there have been significant improvements in power conversion efficiency (PCE) in BHJ solar cells because of the synthesis of specific polymers and small molecules, the achievement of improved nanomorphology through process control (by processing additives), and the use of new architectures (e.g., the inverted structure with specific transport layers).[5–10] The electron-transport layer (ETL) plays an especially important role in enhancing the PCE with increased short-circuit current density (J_{SC}), and fill factor (FF) in the device because of improved charge transport and charge extraction. Moreover, the ETL affects device stability as an oxygen scavenger that can protect against degradation of BHJ in air.[5,11–13]

Graphene is considered a promising conductive, high strength, durable, and thermally stable carbon-based material that is broadly applicable in optoelectronic devices.[14–16] We have devised a method to transfer a graphene film by stamping nanotechnology. Thus, graphene synthesized by chemical vapor deposition (CVD) using a roll-to-roll process can be transferred and deposited onto specific regions of a substrate.[17] Since graphene features high conductivity and excellent transparency, it can be directly used as an electrode in organic emitting diodes and polymer solar cells.[18–20] Although the PCE of polymer solar cells must be improved, the use of graphene as an ETL offers significant advantages to the multilayer anode. Through simulations, we show that graphene oxide based materials, in addition to serving as efficient ETL, can enhance the harvesting of solar energy. Finally, we explore and utilize the tunable work function (WF) of graphene oxide (GO).[21,22] Thus, we find that GO can significantly improve the performance of BHJ solar cells.

[*] Dr. D. H. Wang, Prof. A. J. Heeger
Center for Polymers and Organic Solids
University of California at Santa Barbara
Santa Barbara, CA 93106-5090 (USA)
E-mail: ajhe1@physics.ucsb.edu
J. K. Kim, Prof. J. H. Park
School of Chemical Engineering and SAINT
Sungkyunkwan University
Suwon 440-746 (Republic of Korea)
Prof. J. H. Seo
Department of Materials Physics
College of Natural Science, Dong-A University
840 Hadan 2 dong, Sahagu, Busan 604-714 (Republic of Korea)
Dr. I. Park
Samsung Advanced Institute of Technology, Samsung Electronics
Yongin 446-712 (Republic of Korea)
Prof. B. H. Hong
Department of Chemistry, Seoul National University
Seoul 151-747 (Republic of Korea)

[**] Research at UCSB (including the fabrication and testing of solar cells and the measurements and analysis of the UPS data) was supported by the National Science Foundation (DMR0856060). J.H.P. acknowledges the support from NRF grants (2010-0029321).
Supporting information for this article is available on the WWW under http://dx.doi.org/10.1002/anie.201209999.

We successfully fabricated high-performance poly[N-9′′-heptadecanyl-2,7-carbazole-alt-5,5-(4′,7′-di-2-thienyl-2′,1′,3′-benzothiadiazole)] (PCDTBT):[6,6]-phenyl C_{71} butyric acid methyl ester ($PC_{71}BM$) BHJ solar cells with stretchable GO as the ETL by a stamping process using a transfer film process. The PCE of the device with PCDTBT/$PC_{71}BM$ BHJ solar cells was initially reported to be 5.9%.[4] Herein, we demonstrate improvement in the PCE to 7.5% using the new ETL.

We fabricated the film using several simple steps. First, graphene with a WF of −4.6 eV[15,23] is synthesized by CVD on a copper foil. A thermal-release tape (TRT) is then attached to the copper foil/graphene. Afterward, the copper foil is removed by etchant, and the transfer film is prepared (see Figure S1 in the Supporting Information) and continuously reacted with HNO_3 to synthesize GO. The resulting GO film (thickness of $\approx$1 nm) can be directly applied as the ETL between the BHJ layer and the Al cathode. To induce better contact between the GO layer and the BHJ, we applied a uniform pressure (0.2 MPa) and carried out the stamping process at elevated temperatures (80–90 °C).

The transferred GO ETL improved the J_{SC} and PCE in the BHJ because of efficient electron charge transport and extraction from BHJ to Al cathode, thus causing the series resistance to be reduced compared with the device without the GO layer. Moreover, the device with sequentially deposited GO and conventional titanium oxide (TiO_x) interlayer,[13,24,25] fabricated through stamping and spin-casting exhibits the highest performance demonstrated for PCDTBT:$PC_{71}BM$ BHJ solar cells with PCE = 7.5%. This result originates from the synergistic effect of improved charge transport and enhanced optical field amplitude compared even to devices with single coated TiO_x or GO. The device with the GO ETL also shows long-term stability comparable to that obtained with TiO_x after storage in air for 30 days.[13,24,26]

Figure 1 shows the device schematic and detailed fabrication steps of the PCDTBT:$PC_{71}BM$ BHJ solar cells with the GO/TiO_x ETL. The control-cell structure without the new ETL layer consists of ITO-glass/poly(3,4-ethylenedioxythiophene): poly(styrenesulfonate) (PEDOT:PSS)/BHJ/Al. The GO from the transfer film is well attached to the surface of PCDTBT:$PC_{71}BM$ BHJ (Figure 1a). After detaching the film, the GO layer is transferred and uniformly coated on top of the BHJ (Figure 1b). Then, the TiO_x layer is continuously spin-coated onto the transferred GO (Figure 1c). Figure 1d displays the final structure of BHJ solar cells after Al cathode deposition. A detailed synthesis of GO, fabrication steps of the transfer film, and devices are described in the Experimental Section and in Figure S1 in the Supporting Information.

Figure 2a shows the current density–voltage (J–V) curves of the PCDTBT:$PC_{71}BM$ BHJ solar cells with and without ETLs, such as TiO_x ($\approx$10 nm), GO ($\approx$1 nm), and GO/TiO_x ($\approx$11 nm). The device with TiO_x exhibited a sharply increased PCE of 7.02% with improved $J_{SC} = 12.08\ mA\,cm^{-2}$ and FF = 0.67, compared with the PCE of the control device without an ETL layer, PCE = 5.35% with $J_{SC} = 10.7\ mA\,cm^{-2}$ and FF = 0.58. Because of the well-matched HOMO (8.0 eV)

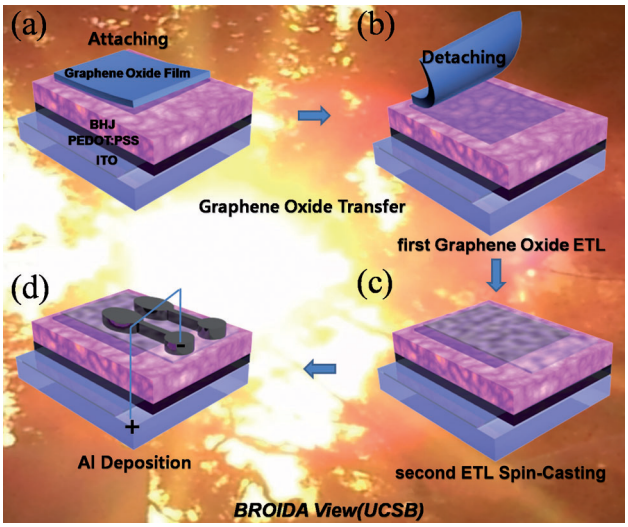

Figure 1. Schematic illustration and fabrication steps of BHJ solar cells with an ETL of graphene oxide (GO) applied by stamping transfer. a) Attachment of the transfer film on top of the BHJ active layer; b) after detachment of the film, the first ETL of GO is uniformly transferred and coated onto the BHJ layer; c) spin-casting of second ETL of TiO_x on top of GO; d) completed device structure after Al deposition.

and LUMO (4.3 eV) levels of TiO_x with the BHJ,[24–25] electron transport and hole blocking is effective during the device operation. Similarly, in case of the device with GO between BHJ and Al cathode, the PCE is 6.72% with enhanced $J_{SC} = 12.36\ mA\,cm^{-2}$ and FF = 0.63 after the stamping process. The improved J_{SC} and PCE are possibly attributed to a reduced electronic charge barrier between BHJ and GO interface. The WF of GO (−4.3 eV)[22] is close to the LUMO level of the fullerene acceptor, thus resulting in efficient electron charge transport.

The surface morphology of PCDTBT:$PC_{71}BM$ BHJ with and without the ETL layers is shown in 3D images obtained by atomic-force microscopy (AFM; Figure 3). The images show uniformly percolated structures and flat surfaces with root-mean-square (rms) roughness values of 0.3–0.7 nm. Interestingly, there is a synergistic effect in BHJ solar cells when the GO and TiO_x are sequentially transferred and spin-coated on top of the BHJ, because of the cascaded energy levels (see Figure S2). Thus, the PCE exhibits the best value of 7.50% (29% increase) with $J_{SC} = 12.40\ mA\,cm^{-2}$ and FF = 0.68 compared with the control cell without any ETL, and with a single ETL: 24% increase with TiO_x, and 18% increase with GO. The data are summarized in Table 1. Moreover, the device with the GO/TiO_x ETL exhibits a reduced series resistance (R_S) of 1.85 $\Omega c\,m^2$ compared with that without ETL

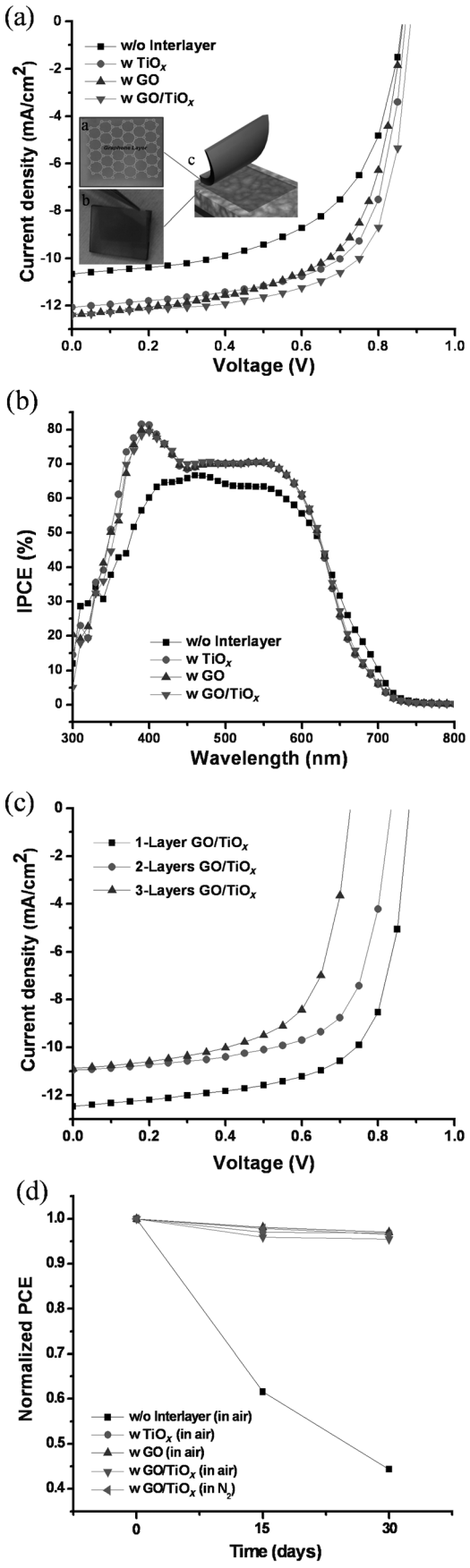

Figure 2. a) *J–V* characteristics, and b) IPCE (in %) of devices from PCDTBT:$PC_{71}BM$ BHJ without an ETL layer and with ETL layers of TiO_x, GO, and GO/TiO_x; c) *J–V* characteristics of the devices with ETLs of one-, two-, and three-layer GO/TiO_x; d) normalized PCE from device-stability test under ambient conditions in air or N_2 atmosphere as a function of time. w/o = without.

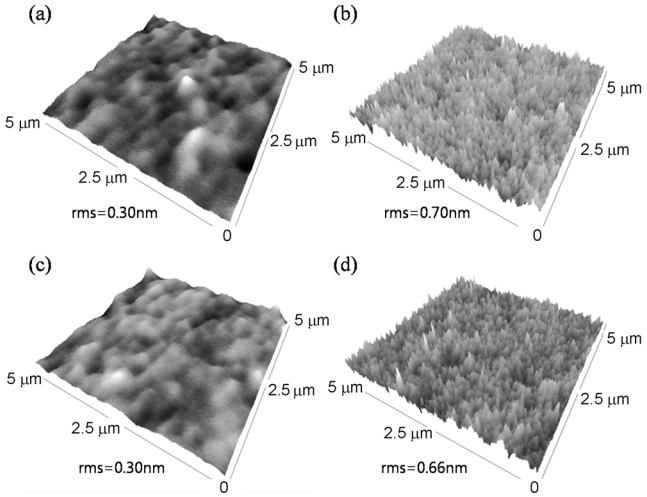

Figure 3. AFM 3D images and rms values of PCDTBT:$PC_{71}BM$ BHJ a) without ETL, b) with TiO_x, c) with GO, and d) with GO/TiO_x interlayers (scan size = 5 μm × 5 μm).

Table 1: Device characteristics of PCDTBT:$PC_{71}BM$ BHJ without ETL, and with ETLs of TiO_x, GO, and GO/TiO_x.

Device structure	V_{OC} [V]	J_{SC} [mA cm^{-2}]	FF	PCE [%]
ITO/PEDOT:PSS/BHJ/Al	0.86	10.66	0.58	5.35
ITO/PEDOT:PSS/BHJ/TiO_x/Al	0.87	12.08	0.67	7.02
ITO/PEDOT:PSS/BHJ/GO/Al	0.86	12.36	0.63	6.72
ITO/PEDOT:PSS/BHJ/GO/TiO_x/Al	0.88	12.40	0.68	7.50

(where $R_s = 2.54\ \Omega cm)^2$, $R_s = 2.50\ \Omega c m^2$ with TiO_x, and $R_s = 2.04\ \Omega c m^2$ with GO. The reduced R_s is well correlated with the enhanced J_{SC}. The high shunt resistance (R_{sh}) was obtained in the device with GO compared to the device without the interlayer (see the *J*–*V* curves at the dark current shown in Figure S3). Therefore, the GO layer plays an important role in reducing R_S and increasing R_{sh}, both of which cause improvement in the PCE. The average PCE values and PCE deviation of the devices without interlayers, with TiO_x, with GO, and with GO/TiO_x were calculated from more than ten devices (Figure S4) to demonstrate the reproducibility.

Figure 2b shows the incident photocurrent conversion efficiency (IPCE) corresponding to the *J*–*V* characteristics of Figure 2a. To confirm the ETL effect of GO in the BHJ solar cells, we selected the well known P3HT:PCBM system. As shown in Figure S5, the device with GO also plays a role of ETL because of the same tendency of enhanced J_{SC} and PCE (11% increase) compared to the device without GO.

To confirm the thickness dependence of the GO in the BHJ solar cells, the layer-by-layer transfer of GO (one-layer, tow-layers, and three-layers) is used by sequential transfer onto the BHJ. The device with single transferred GO/TiO_x exhibits best average PCE of 7.43% (open-circuit voltage (V_{OC}) = 0.88, $J_{SC} = 12.46$ mA cm^{-2}, FF = 0.68) while two-layer GO/TiO_x and three-layer GO/TiO_x show gradually decreasing PCE of 6.13% ($V_{OC} = 0.83$, $J_{SC} = 10.95$ mA cm^{-2}, FF = 0.67), and 5.06% ($V_{OC} = 0.73$, $J_{SC} = 10.89$ mA cm^{-2}, FF = 0.64), respectively, as shown in Figure 2c and by the IPCE in Figure S6. Thus, the sequential transfer has a negative effect on the PCE of the devices because of the reduced V_{OC}, which possibly originates from unstable contact between the GO layers. Furthermore, the thick GO will lead to an increased R_S in the device.[5] Therefore, optimized thickness and good contact of the GO layer are important factors required to obtain high-performance solar cells.

The BHJ devices with GO as the ETL exhibit higher long-term stability with low efficiency decay when stored in air or N_2 compared with the device without the ETL layer (see normalized PCE data in Figure 2d). After 30 days, the device without an ETL layer shows a sharp efficiency decay of 56%. However, BHJ devices fabricated with GO and GO/TiO_x exhibit relatively high stability; the PCE is reduced by only 3–4% after storage in air for 30 days (see Table S1). Thus, the GO layer prevents the degradation of the device and offers the promise of long-term operation similar to that observed with TiO_x as the ETL.[13,24–26]

In order to clarify the influence of ETL layers on energy-level alignment, ultraviolet photoelectron spectroscopy (UPS) was employed. Figure 4a shows the UPS spectra for the PCDTBT/$PC_{71}BM$ films without interlayer (solid line) and with interlayers (dashed/dotted lines). An examination of the secondary electron cutoff (E_{SE}) region (14–18 eV; Figure 4a, left) shows a shift in the vacuum level (E_{vac}), which is affected by the magnitude of the interfacial dipole.[27–31] After deposition of TiO_x, GO, and GO/TiO_x ETL layers, respectively, on the BHJ, the shifts in the E_{SE} between the BHJ layer and ETL layers changed significantly. The strongest interfacial dipole was observed for the BHJ/GO/TiO_x interface, while the BHJ/GO interface exhibited the weakest interfacial dipole.

The highest-occupied molecular orbital (HOMO) energy levels (E_{HOMO}) were determined from the low binding energy region (0–4 eV; Figure 4a, right). The energy difference between E_{HOMO} and the zero binding energy corresponds to the hole injection barrier (Φ_h) in BHJ devices. Energy level diagrams for the BHJ films with and without the ETL layers are generated by the UPS data (Figure 4b–e). The Φ_h for PCDTBT/$PC_{71}BM$ without ETL layer is 0.40 eV relative to the WF of ITO/PEDOT:PSS. When TiO_x and GO interlayers were introduced, the Φ_h values were increased from 0.40 eV to 0.87 eV and 0.73 eV, respectively. The anticipated electron injection barrier can be estimated by the difference between the Fermi level (E_F) and the LUMO of the ETL layers, as obtained by considering the UPS-determined HOMO energy level and the optical gap. The results indicate an increased Φ_h and thereby show that electron injecton barrier decreases after introducing the ETL layers. Thereby, an increased Φ_h is caused by downward shift of E_{vac}, which can lead to a smaller electron injection barrier in BHJ systems with ETL layers. Since the GO layer is located beneath the cathode, the electrons would transport more efficiently from the bulk of BHJ to the cathode, which is similar to the previously demonstrated role of TiO_x.[24–26] Moreover, a synergistic effect is estimated in BHJ devices with the sequentially coated GO and TiO_x interlayer because of the significant decrease in

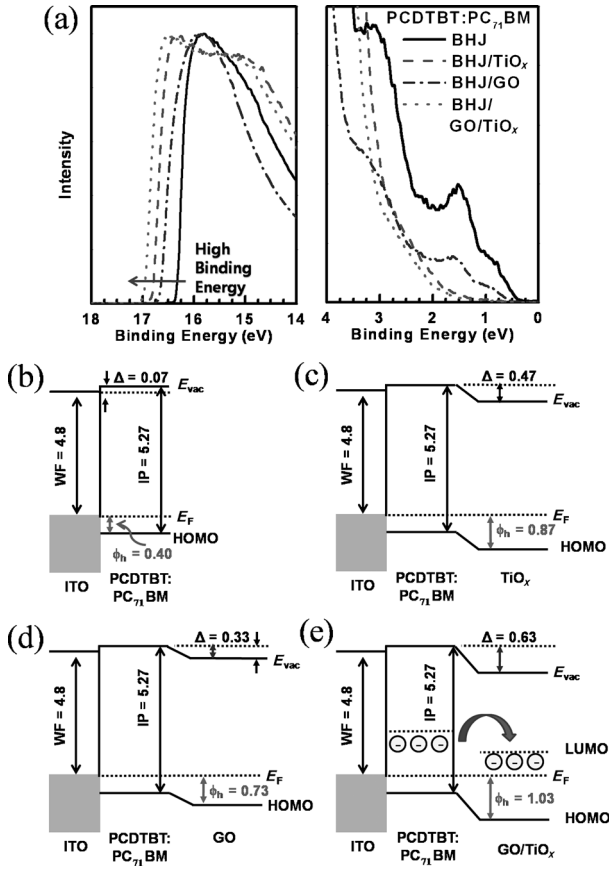

Figure 4. a) UPS spectra of PCDTBT:PC_{71}BM BHJ without and with ETL. b–e) Energy-level diagrams of BHJ films without ETL (b), and with ETLs of TiO_x (c), GO (d), and GO/TiO_x (e). E_{vac} = vacuum level, E_F = Fermi level, Δ = interfacial dipole, Φ_h = hole-injection barrier.

electron injection barrier from 1.50 eV to 0.87 eV (Figure S7). The downshift of E_{vac} is suggested as the origin of the reduced electron injection barrier and accounts for the improved J_{SC} and PCE.

Finally, we carried out a simulation analysis of optical electric field distribution as a function of wavelength in the BHJ devices without and with the TiO_x, GO, GO/TiO_x layers, respectively (Figure 5). For carrying out the simulations, the optical parameters of materials such as absorption constant and refractive index were obtained from previous reports.[32–34] According to the results, the optical electric field amplitude is slightly enhanced for the device with GO as the ETL compared with the device without the GO layer, and reduced relative to the device with the TiO_x layer (Figure 5a–c). Furthermore, we found a synergistic effect of the device with GO/TiO_x (Figure 5d). The highest optical electric field amplitude for incident light wavelength of 500 nm and 600 nm are 1.02 $V m^{-1}$ and 3.57 $V m^{-1}$, respectively. The data of devices with TiO_x (500 nm: 0.94 $V m^{-1}$, and 600 nm: 3.49 $V m^{-1}$) and TiO_x/GO are compared in Figure 5b and d. The maximum optical electric field amplitudes of the devices with and without ETL layers on the BHJ active layer are summarized in Table S2. The variation of optical electric field amplitudes of BHJ solar cells correlates with the J_{SC} and PCE values. The enhanced J_{SC} originates from the high electric field amplitude in BHJ active layer which generates more photocurrent in the devices.[35] According to the simulation, we conclude that inserting GO leads to BHJ solar cells with enhanced electric field amplitudes compared with similar cells without ETL layers. Moreover, the highest optical electric field distribution of the device with GO/TiO_x is correlated with the best PCE and J_{SC} (with the added benefit of reduced series resistance and improved electron charge transport).

In summary, we successfully fabricated high-performance PCDTBT:PC_{71}BM BHJ solar cells comprising an electron charge-transport layer of stretchable GO by stamping transfer. By utilizing the transfer film, the GO can be directly used and coated onto the BHJ surface through the stamping process. The GO ETL plays an important role in improving J_{SC} and PCE (18% increase) in BHJ solar cells compared with solar cells without interlayer. Furthermore, the device with ETL of GO/TiO_x exhibits the highest PCE of 7.50% (29% increase). Another dominant effect is improved electric field amplitude in the devices from optical simulation. Thus, "cavity effects" implied by the simulations cause increases in the J–V characteristics (V_{OC}, J_{SC}, and FF). Furthermore, the device with GO (3% PCE decay) exhibits high stability compared with the device without interlayer (56% PCE decay); a result that is comparable to that obtained from TiO_x after storage for 30 days in air. The BHJ solar cell with transferable GO as ETL is an encouraging architecture for achieving high-performance devices with an ETL inserted by stamping nanotechnology.

Experimental Section

Synthesis of graphene oxide (GO) and fabrication of transfer films: Graphene was deposited on a copper foil by CVD (chemical vapor deposition). The copper foil was inserted into a tubular quartz chamber followed by annealing at 1000 °C with a flow of 8 s.c.c.m (standard cubic centimeter per minute) H_2 at 90 mtorr for 30 min. After 24 s.c.c.m. of CH_4 and 8 s.c.c.m. of H_2 were flowed through the chamber at 460 mtorr for 30 min, the chamber was cooled to room temperature with a flow of H_2 under a pressure of 90 mtorr.[15]

As-synthesized graphene on the copper foil was exploited by the following steps. Thermal-release tape (TRT), composed of an adhesive polymer-coated polyethylene terephthalate (PET) film,[36,37] was covered with the graphene layer and uniformly attached to the layer by a roll-to-roll process. Subsequently, the sample was chemically treated with 100 mM ammonium persulphate solution ($(NH_4)_2S_2O_8$) for 3 h to remove the copper foil. After rinsing out possible residues with deionized water, the graphene layer was immersed in HNO_3 to be oxidized.[22] Then, the graphene oxide (GO) layer was stamped on a target substrate. To fully transfer the GO from the polymer film (mother substrate) to the surface of the target substrate, the back side of the graphene/polymer film on top of the hot plate was treated with pressure (0.2 MPa) and heat (80–90 °C). Because of the uniform force and the applied heat, the GO on the polymer film was successfully and reproducibly transferred and deposited on the counter substrate after detaching the film.

Fabrication of solar cells: The ITO glass was prepared by a cleaning process using detergent, acetone, and isopropyl alcohol with ultrasonication. Then, the ITO was exposed to UV-ozone (20 min) to reform the surface, and the hole transport material of poly(3,4-ethylenedioxythiophene):poly(styrenesulfonate)

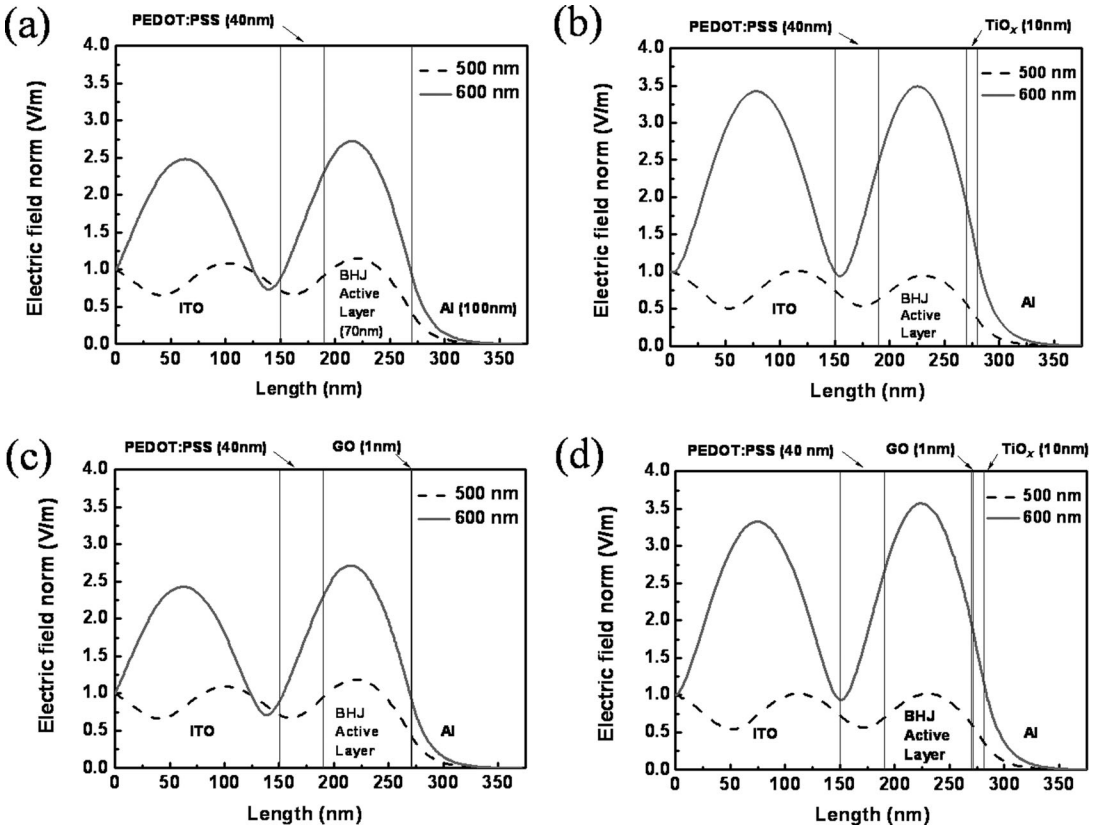

Figure 5. Simulated distribution of the normalized optical electric field for light inside BHJ devices as a function of wavelength: glass-ITO (150 nm)//PEDOT:PSS (40 nm)//PCDTBT:$PC_{71}BM$ BHJ (70 nm)//ETL//Al (100 nm), a) without ETL, b) with TiO_x ($\approx$10 nm), c) with GO ($\approx$1 nm), d) with GO/TiO_x ($\approx$11 nm).

(PEDOT:PSS; Clevious PH) was spin-coated (5000 rpm, for 40 s) on the ITO with a thickness of around 40 nm. The PEDOT:PSS-coated ITO was dried at 140 °C for 10 min. It was then moved to a glove-box to spin-cast the PCDTBT:$PC_{71}BM$ BHJ active layer with a thickness of $\approx$70 nm (6000 rpm, 40 s). The BHJ solution with a total blend ratio of PCDTBT/$PC_{71}BM$ = 7 mg:28 mg was prepared by dissolving in a solvent mixture of DCB/CB = 3:1 (1 mL).[4,7,9] The solution was stirred continuously at 250 rpm and 60 °C on a hotplate overnight. The BHJ active layer was dried at 80 °C for 10 min, and then the conventional electron-transport layer (ETL), TiO_x, GO, and GO/TiO, was coated by spin-casting, stamping transfer, or the combined process. Finally, the Al cathode (thickness of 100 nm) was deposited by thermal evaporator under a vacuum pressure of 4×10^{-6} torr. The devices were encapsulated by a cleaned cover glass and a UV-curable epoxy in the N_2-filled glove box.

Measurement and characterization: After calibration of the light source using silicon reference cells with an AM 1.5 Global solar simulator, the encapsulated BHJ solar cells were measured by a Keithley 236 source unit during the exposure of the devices to an intensity of 100 mW cm^{-2}. Then, the *J–V* curves and PCE parameters (V_{OC}, J_{SC}, and FF) were obtained. To determine the exact cell areas, we used the aperture of 11.76 mm^2 on top of the deposited Al cathode during the measure. The morphology and surface roughness of BHJs with and without interlayers were determined by atomic-force microscopy (AFM; Veeco, USA; D3100) to confirm the contact of interlayers. The IPCEs were investigated by a QE measurement system (PV measurements, Inc.) after the calibration of monochromatic power density to check and match with the *J–V* characteristics.

For the UPS analysis, the PCDTBT:$PC_{71}BM$ (1:4) BHJ dissolved in DCB/CB (3:1) (total: 35 mg/1 mL) was spin-cast on the ITO-glass substrate. The films were dried at 80 °C for 10 min. The TiO_x, GO, and GO/TiO_x layers were then spin-coated and transferred on top of BHJ films. The UPS analysis chamber was equipped with a hemispherical electron-energy analyzer (Kratos Ultra Spectrometer), and was maintained at 1.33×10^{-7} Pa. UPS measurements were carried out using the He I ($h\nu$ = 21.2 eV) source. The electron-energy analyzer was operated at a constant pass energy of 10 eV (for UPS). During UPS measurements, a sample bias of −9 V was used in order to separate the sample and the secondary edge for the analyzer.

Received: December 14, 2012
Published online: January 22, 2013

Keywords: electron transport · graphene oxide · nanotechnology · solar cells · stamping transfer

[1] N. S. Sariciftci, L. Smilowitz, A. J. Heeger, F. Wudl, *Science* **1992**, *258*, 1474–1476.
[2] G. Yu, J. Ga, J. C. Hummelen, F. Wudl, A. J. Heeger, *Science* **1995**, *270*, 1789–1791.
[3] A. J. Heeger, *Angew. Chem.* **2001**, *113*, 2660–2682; *Angew. Chem. Int. Ed.* **2001**, *40*, 2591–2611.
[4] S. H. Park, A. Roy, S. Beaupré, S. Cho, N. Coates, J. S. Moon, D. Moses, M. Leclerc, K. Lee, A. J. Heeger, *Nat. Photonics* **2009**, *3*, 297–303.
[5] Z. He, C. Zhong, S. Su, M. Xu, H. Wu, Y. Cao, *Nat. Photonics* **2012**, *6*, 591–595.
[6] L. Dou, J. You, J. Yang, C.-C. Chen, Y. He, S. Murase, T. Moriarty, K. Emery, G. Li, Y. Yang, *Nat. Photonics* **2012**, *6*, 180–185.

[7] D. H. Wang, D. Y. Kim, K. W. Choi, J. H. Seo, S. H. Im, J. H. Park, O. O. Park, A. J. Heeger, *Angew. Chem.* **2011**, *123*, 5633 – 5637; *Angew. Chem. Int. Ed.* **2011**, *50*, 5519 – 5523.
[8] Z. He, C. Zhong, X. Huang, W.-Y. Wong, H. Wu, L. Chen, S. Su, Y. Cao, *Adv. Mater.* **2011**, *23*, 4636 – 4643.
[9] D. H. Wang, J. S. Moon, J. Seifter, J. Jo, J. H. Park, O. O. Park, A. J. Heeger, *Nano Lett.* **2011**, *11*, 3163 – 3168.
[10] C. E. Small, S. Chen, J. Subbiah, C. M. Amb, S.-W. Tsang, T.-H. Lai, J. R. Reynolds, F. So, *Nat. Photonics* **2012**, *6*, 115 – 120.
[11] J. You, C.-C. Chen, L. Dou, S. Murase, H.-S. Duan, S. A. Hawks, T. Xu, H. J. Son, L. Yu, G. Li, Y. Yang, *Adv. Mater.* **2012**, *24*, 5267 – 5272.
[12] M. Jørgensen, K. Norrman, S. A. Gevorgyan, T. Tromholt, B. Andreasen, F. C. Krebs, *Adv. Mater.* **2012**, *24*, 580 – 612.
[13] D. H. Wang, S. H. Im, H. K. Lee, O. O. Park, J. H. Park, *J. Phys. Chem. C* **2009**, *113*, 17268 – 17273.
[14] X. Li, W. Cai, J. An, S. Kim, J. Nah, D. Yang, R. Piner, A. Velamakanni, I. Jung, E. Tutuc, S. K. Banerjee, L. Colombo, R. S. Ruoff, *Science* **2009**, *324*, 1312 – 1314.
[15] S. Bae, H. Kim, Y. Lee, X. Xu, J.-S. Park, Y. Zheng, J. Balakrishnan, T. Lei, H. R. Kim, Y. I. Song, Y.-J. Kim, K. S. Kim, B. Özyilmaz, J.-H. Ahn, B. H. Hong, S. Iijima, *Nat. Nanotechnol.* **2010**, *5*, 574 – 578.
[16] S. Bhaviripudi, X. Jia, M. S. Dresselhaus, J. Kong, *Nano Lett.* **2010**, *10*, 4128 – 4133.
[17] K. S. Kim, Y. Zhao, H. Jang, S. Y. Lee, J. M. Kim, K. S. Kim, J.-H. Ahn, P. Kim, J.-Y. Choi, B. H. Hong, *Nature* **2009**, *457*, 706 – 710.
[18] J. Wu, M. Agrawal, H. A. Becerril, Z. Bao, Z. Liu, Y. Chen, P. Peumans, *ACS Nano* **2010**, *4*, 43 – 48.
[19] Z. Liu, J. Li, Z.-H. Sun, G. Tai, S.-P. Lau, F. Yan, *ACS Nano* **2012**, *6*, 810 – 818.
[20] C.-L. Hsu, C.-T. Lin, J.-H. Huang, C.-W. Chu, K.-H. Wei, L.-J. Li, *ACS Nano* **2012**, *6*, 5031 – 5039.
[21] C. X. Guo, G. H. Guai, C. M. Li, *Adv. Energy Mater.* **2011**, *1*, 448 – 452.
[22] T. H. Han, Y. Lee, M. R. Choi, S. H. Woo, S. H. Bae, B. H. Hong, J. H. Ahn, T. W. Lee, *Nat. Photonics* **2012**, *6*, 105 – 110.
[23] Y.-J. Yu, Y. Zhao, S. Ryu, L. E. Brus, K. S. Kim, P. Kim, *Nano Lett.* **2009**, *9*, 3430 – 3434.
[24] J. Y. Kim, S. H. Kim, H.-H. Lee, K. Lee, W. Ma, X. Gong, A. J. Heeger, *Adv. Mater.* **2006**, *18*, 572 – 576.
[25] J. Y. Kim, K. Lee, N. E. Coates, D. Moses, T.-Q. Nguyen, M. Dante, A. J. Heeger, *Science* **2007**, *317*, 222 – 225.
[26] K. Lee, J. Y. Kim, S. H. Park, S. H. Kim, S. Cho, A. J. Heeger, *Adv. Mater.* **2007**, *19*, 2445 – 2449.
[27] Y. Gao, *Acc. Chem. Res.* **1999**, *32*, 247 – 253.
[28] H. Ishii, K. Sugiyama, E. Ito, K. Seki, *Adv. Mater.* **1999**, *11*, 605 – 625.
[29] I. G. Hill, D. Milliron, J. Schwartz, A. Kahn, *Appl. Surf. Sci.* **2000**, *166*, 354 – 362.
[30] S. Braun, W. R. Salaneck, M. Fahlman, *Adv. Mater.* **2009**, *21*, 1450 – 1472.
[31] J. H. Seo, R. Yang, J. Z. Brzezinski, B. Walker, G. C. Bazan, T.-Q. Nguyen, *Adv. Mater.* **2009**, *21*, 1006 – 1011.
[32] A. J. Moulé, J. B. Bonekamp, K. Meerholz, *J. Appl. Phys.* **2006**, *100*, 094503.
[33] H. Hänsel, H. Zettl, G. Krausch, R. Kisselev, M. Thelakkat, H.-W. Schmidt, *Adv. Mater.* **2003**, *15*, 2056 – 2060.
[34] K. Fehse, K. Walzer, K. Leo, W. Loevenich, A. Elschner, *Adv. Mater.* **2007**, *19*, 441 – 444.
[35] W. H. Lee, S. Y. Chuang, H. L. Chen, W. F. Su, C. H. Lin, *Thin Solid Films* **2010**, *518*, 7450 – 7454.
[36] Y. Lee, S. Bae, H. Jang, S. Jang, S.-E. Zhu, S. H. Sim, Y. I. Song, B. H. Hong, J.-H. Ahn, *Nano Lett.* **2010**, *10*, 490 – 493.
[37] J. D. Caldwell, T. J. Anderson, J. C. Culbertson, G. G. Jernigan, K. D. Hobart, F. J. Kub, M. J. Tadjer, J. L. Tedesco, J. K. Hite, M. A. Mastro, R. L. Myers-Ward, C. R. Eddy, Jr., P. M. Campbell, D. K. Gaskill, *ACS Nano* **2010**, *4*, 1108 – 1114.

